

# **Novel Curve-Shape Sandwich Composites with Flexible Cores for Rehabilitation of Buried Infrastructure: Experimental and Analytical Studies Considering Geometric Non-Linearity**

Anita Shiny Kanagaraj<sup>1</sup> and Pedram Sadeghian<sup>2</sup>

## **Abstract:**

This paper presents findings from an experiment examining a novel curve-shape sandwich composites made of fiber-reinforced polymer (FRP) facesheets and flexible cores under transverse compressive loading. The curve-shape sandwich composites aim to enhance strength and stiffness while minimizing material use, particularly as liner for rehabilitation of large, buried infrastructure like pipes and culverts. The study involved fabricating and testing 24 circular liners with various facesheet-core combinations. Results include deflection measurements, load data, and tensile strain values at different points on the liners. The stiffness of each sandwich specimen was compared to theoretical predictions based on composite facesheet behavior. Notably, bulkermat cores demonstrated superior stiffness and strength compared to 3D woven fabric cores, exhibiting higher composite action. In contrast, solid-wall liners exhibited greater deformations than sandwich liners. To predict these significant deformations, an iterative analytical model was developed, accounting for geometric non-linearity. This model accurately predicted test data prior to any material non-linearity, such as facesheet or core failure. Additionally, the model was used

---

<sup>1</sup> Former MASC Student, Department of Civil and Resource Engineering, Dalhousie University, Canada. Currently Structural Engineer in Training, Hatch Ltd., Saskatoon, Saskatchewan, Canada.

<sup>2</sup> Associate Professor and Canada Research Chair in Sustainable Infrastructure, Department of Civil and Resource Engineering, Dalhousie University, Halifax, Nova Scotia, Canada (Corresponding Author). Email: [Pedram.Sadeghian@dal.ca](mailto:Pedram.Sadeghian@dal.ca)

to perform a parametric analysis, exploring various liner characteristics, including diameter, FRP layers, core thickness, and liner shape.

DOI: <https://doi.org/10.1061/JPSEA2.PSENG-1594>

**Keywords:** FRP; composite; liner; sandwich; test; model; non-linearity.

## **INTRODUCTION**

Large diameter underground pipes have found diverse applications in the modern society. They are primarily used as culverts, storm water drains, sewers, water conduits, storage tanks and tunnels. These pipes are often made from concrete and tend to deteriorate as they age due to their exposure to various physical and chemical parameters like soil pressure, pressure of conveyed materials, chemical attacks, freeze and thaw action, and corrosion. Thereby, a reduction in the strength, durability and service life of the structure can be observed. Various trenchless rehabilitation methods such as slip lining, cured-in-place pipe (CIPP) lining, pipe jacking, fold and reformed piping, pipe bursting, and spot repair have been widely used to reline and improve the life of such deteriorated pipes (Syachrani et al. 2010, Simpson et al. 2017, Zhao and Rajani 2010). Techniques like slip lining has a popularity index (PI) of 93.2% and CIPP lining has a PI of 75% in the United States (Syachrani et al. 2010, Simpson et al. 2017) and have been used to rehabilitate a broad range of pipes/culverts. Alternatively, hand lay-up method of FRP lining has been considered effective to rehabilitate deteriorated pipes with large diameters (Abraham and Gillani 1999, Walsh 2017, Lee and Karbhari 2005), for which they are bonded with FRP liners on the inside. FRP composites are highly preferred for this purpose because of their high strength-to-weight ratio (specific strength), dimensional stability, anti-corrosion, low installation and maintenance cost, durability over a range of imposed conditions and good mechanical properties (Rafiee 2016, Park et al. 2014, Rafiee and Habibagahi 2018a and 2018b). The most prominent

aspect of these materials is the smoothness they provide inside the pipe section. Smoothness directly translates to less friction, which resists the scale deposits and therefore the efficiency of pipe flow is increased. Unlike many conventional rehabilitation techniques which have an inconsistent surface finish and decreased flow area, FRP liners provide a minimal or no reduction in flow capacity across the pipe.

Solid-wall FRP liners can be used for the rehabilitation of existing concrete or prestressed concrete pipes. These could either be unidirectional or bidirectional fabrics. Based on design requirements, one or more layers of the fabric can be applied to achieve an adequate strength and stiffness in the desired direction. Fabric strips from 300 to 1500 mm wide rolls are applied in the hoop direction multiple times determined by the engineer. The ends of the fabric are butt jointed with the adjacent fabric, along the length of the pipe to ensure the development of full strength of fibres in that direction. Bidirectional fabrics can be also manufactured with different amounts of fibers oriented in both longitudinal and lateral directions (Karbhari 2015, Karbhari and Seible 2000, Aylor and Hirtz 1990). In both cases, care must be taken to properly align the fibers to achieve the required structural capacity.

Various studies on the behavior of solid-wall FRP pipes, under axial loading and/or internal hydrostatic pressure (Das and Baishya 2016, Wang et al. 2016), impact loading (Wakayama et al. 2002, Deniz et al. 2013) and fatigue cycles (Tarakcioglu et al. 2007, Rafiee and Elasmî 2017), pipe mechanics and fracture strength (Parashar and Mertiny 2011) have been carried out. To understand the behavior of solid-wall FRP liners, tests such as sectional ring tests, external load test for three-edge bearing (TEB) strength, full scale hydrostatic burst test, compressive transverse loading test have been conducted (Lee and Karbhari 2005, Rafiee 2016, Houssam and Sean 2001). The use of multiple layers of FRPs is usually needed to gain the required moment of inertia and stiffness for

a solid-wall liner. Using multiple layers increases the cost and extends the duration of rehabilitation work. To overcome these shortcomings, including an inexpensive layer in the middle of the liner can be used to form a sandwich composite liner providing adequate moment of inertia, stiffness, and strength instead of a solid-wall liner (Karbhari 2015). Sandwich liners can have very thin but tough facesheets and a lightweight, low-density core providing high flexural stiffness and strength as the core separates the two facesheets and thereby increasing the distance between them to produce an increased moment of inertia (McCracken and Sadeghian 2018a and 2018b, Betts et al. 2018, Allen 2013). Compressive and tensile stresses due to bending are resisted by the FRP facesheet, while shear stresses are resisted by the core material. The bending stiffness and strength of such structurally aligned sandwich liners are much larger than that of a solid wall liner of same total weight made of the same materials as the facesheets, which makes them preferable for high performance structural rehabilitation (Zinno et al. 2010). Since sandwich liners can be custom made with flexible skin and core rolls, they can fit into any shape of the cross-section of deteriorated pipe or culvert. One of the earliest sandwich liners put to practical application includes a honeycomb-FRP liner that uses either glass or carbon facesheets and a polypropylene honeycomb as core. Using this sandwich liner of 10 mm thickness, the stiffness was improved up to 37 times of a solid-wall liner of the same thickness with only an increase of 9% in weight (Karbhari 2015).

Based on the literature, it is evident that innumerable studies have been performed to understand the properties of prefabricated sandwich pipes. These pipes are mainly used for under sea and deep-water applications. Studies on material properties (Liu et al. 2017, Hansen 1998), lateral buckling (Wang et al. 2017), shear deformation (Jianghong et al. 2015), external pressure capacity (Arjomandi and Taheri 2011), elastic buckling and bending capacity (Arjomandi and Taheri 2010, 2012) have been performed based on experimental, analytical, and numerical

approaches. Sandwich pipes of different facesheet-core-resin combinations have been patented with some providing the method of fabrication as well (Kittson and Kulawic 1998, Imoto et al.1993, Aylor and Hirtz 1990). Recently, Ehsani (2017) has developed the concept of premanufactured sandwich liners and implemented the system in field applications and showed that the use of liners reduced the repair time significantly.

Despite of multiple studies on the behavior of prefabricated sandwich pipes, the behavior of sandwich liners using a wet lay-up technique is not well known. Further studies need to be conducted for different core materials. Also, no simple analytics have been developed to explain the geometric non-linearity displayed by the liners as they largely deform under loading.

In this study, thin solid-wall liners and sandwich liners were fabricated. The solid-wall liners were made of glass FRP (GFRP) or carbon FRP (CFRP). Likewise, sandwich liners consisted of GFRP or CFRP facesheets were fabricated using two different flexible core materials (namely, 3D woven fabric or bulkermat core). The liners were tested under the parallel-plate compression loading according to ASTM D2412 (2021) to study their stiffness, behavior, and failure. Also, an analytical model was developed using an iterative procedure based on the geometric non-linearity of the liners to find the large deformations observed in the tests.

## **RESEARCH SIGNIFICANCE**

Buried infrastructures are prone to deterioration as they age due to many physical, chemical, biological, and environmental factors. The failure of a deteriorated pipe or culvert can cause disruption to the traffic, widespread pollution, local flooding, emission of harmful gasses etc. Using FRP composites to rehabilitate such pipes have proven to be a viable solution. Although they are effective, using multiple layers of FRP fabrics to attain a required strength and stiffness can be very expensive. This research is therefore intended to efficiently use thin curve-shape

sandwich composites as liner for rehabilitation of aging buried infrastructure like large diameter water or wastewater systems and culverts. Previous studies have suggested that thin-walled sandwich composites are ideal for rehabilitation of curved surfaces (MacDonnell and Sadeghian 2020, Ehsani 2017). Since the dry fabrics come in a roll, it is easier to transport and work with and the cores being flexible, can take the shape of the existing structure unlike honeycomb cores, which are rigid. To have an understanding about the structural behavior of these liners under loading, it is important to have proper analytical tools. Based on the literature, it is evident that appropriate tools to contemplate the performance characteristics and the failure mechanism of loaded liners are not available. This study has attempted to generate an iterative analytical model that can encapsulate the concept of geometric linearity as the liner with circular cross-section starts deforming elliptically. The results of this research can lead to design of a cost-effective rehabilitation system for aging buried infrastructure.

## **EXPERIMENTAL PROGRAM**

### **Test Matrix**

A total of 24 thin-walled liners were fabricated to be tested under the parallel-plate compression loading method as shown in Figure 1. The specimens were divided into six groups of two solid-wall and four sandwich liners. Table 1 summarizes the details and dimensions of the specimen groups. The solid-wall liner specimens were used as control cases made of four layers of either GFRP or CFRP composites. For the sandwich liners, two layers of either GFRP or CFRP facesheets were used at each side of a flexible thin core made of either a 3D woven fabric or bulkermat core. The solid-wall specimens were identified with a specimen ID as XY, where X stands for the number of fabric layers and Y stands for either glass (G) or carbon (C) fiber. For example, 4G stands for a solid-wall specimen with 4 layers of GFRP. The sandwich specimens

were identified with a specimen ID as XY-Z-XY, where X stands for the number of fabric layers per facesheet, Y stands for either glass (G) or carbon (C) fiber, Z stands for either the 3D woven fabric core (W) or the bulkermat core (B). For example, 2G-W-2G stands for a sandwich specimen with 2 layers of GFRP per facesheet and a 3D woven fabric core. Four identical specimens per specimen group were manufactured.

### **Material Properties**

**Resin:** A two-component epoxy resin with the mixed ratio of 2:1 by volume (two parts of resin and one part of hardener) was used. After the full cure time of 48 hours, the resin matrix was reported to have a tensile strength, compressive strength, and flexural strength of 49.3 MPa, 65.4 MPa and 76.8 MPa, respectively. The tensile modulus, compressive modulus, and flexure modulus of the resin matrix were 2.00 GPa, 3.25 GPa, and 1.74 GPa, respectively, as specified by the manufacturer (QuakeWrap Inc., Tucson, AZ, USA).

**GFRP:** For making GFRP composites, a unidirectional glass fabric with the aerial weight of 915 g/m<sup>2</sup> was used. The glass fibers of the fabric had the tensile strength of 3.24 GPa, tensile elastic modulus of 72.4 GPa, and rupture strain of 4.5% as specified by the manufacturer. When the glass fabric was laminated with the epoxy, the tensile strength and elastic modulus of GFRP was of 583 MPa and 21.75 GPa, respectively, based on the ply thickness of 1.3 mm (McCracken and Sadeghian 2018b).

**CFRP:** For making CFRP composites, a unidirectional carbon fabric with the aerial weight of 943 g/m<sup>2</sup> was used. The carbon fibers of the fabric had the tensile strength of 3.8 GPa, tensile modulus of 231 GPa, and rupture strain of 1.64% as specified by the manufacturer. When the glass fabric was laminated with the epoxy, the tensile strength and elastic modulus of CFRP was of 930 MPa

and 89.60 GPa, respectively, based on the ply thickness of 1.24 mm (McCracken and Sadeghian 2018b).

**Woven Fabric Core:** Two types of flexible core materials were used in this study, namely a 3D woven fabric core and a bulkermat core. The 3D woven fabric was made of two bi-directionally woven glass fabrics, mechanically integrated with vertical woven piles. One pillar had two S-shaped piles and appeared in shape of 8 and 1 from the warp and weft direction, respectively. The dry aerial weight and thickness of the core was  $1050 \text{ g/m}^2$  and 8 mm. The density in the warp direction was 15 ends/cm and density in weft direction was 8 ends/cm. The tensile strength in warp and weft directions were specified to be 6000 N/50 mm and 10000 N/50 mm, respectively, as specified by the manufacturer. Based on preliminary tests carried out by McCracken and Sadeghian (2018b), the average thickness of the 3D woven fabric core after saturating with the epoxy resin and curing was 7.54 mm and the weight of the core was  $2988 \text{ g/m}^2$ .

**Bulkermat Core:** The bulkermat was a low density, nonwoven continuous-strand laminate bulker/print control mat constituting of micro balloons (45% by weight). It had a density of  $0.045 \text{ g/m}^3$ , dry aerial weight of  $160 \text{ g/m}^2$  and dry thickness of 4.1 mm. The tensile strength and elastic modulus in the longitudinal and transverse directions were 6.4 and 5.0 MPa, and 1.2 and 1.0 GPa, respectively. Material properties of fabrics, epoxy, and core material were reported as specified by the manufacturer. Based on tests conducted by MacDonnell and Sadeghian (2020), the elastic modulus and shear strength of the cured resin-impregnated bulkermat was determined to be 374 MPa and 2.2 MPa, respectively.

### **Specimen Fabrication**

While producing the liner specimens, sheets of glass and carbon fabric and the 3D woven fabric and bulkermat core, were cut to the required length using shears. Cutting out large dimension

sheets, helped in fabricating a long pipe-shape (liner) specimen at once and then cutting it into 4 liners segment specimens. The wet lay-up method was used to fabricate all the specimens. The fabric was thoroughly cleaned of any minute dust particles. A plastic sheet was used to cover a cardboard mandrel before placing the fabric. For the solid-wall liners, a layer of resin was applied on the plastic sheet for good bonding and then four layers of glass or carbon fabric was wrapped around while sufficiently wetting the fabric with epoxy, with an end overlap of 100 mm. A roller was used to evenly distribute the resin over the fabric surface and a spatula was used to smoothen the resin layer. Similarly, for the sandwich liners, 2 layers of glass or carbon fabric were applied as the inner and outer facesheets and one layer of the 3D woven fabric or bulkermat were applied as the core to make the liners. A motor system was used to spin the mandrel slowly to create a small centrifugal force, to avoid the concentration of the resin at the bottom. The specimens cured for approximately 24 hours at room temperature with a plastic sheet covering its exposed surface, to obtain a smooth surface, then the cardboard mould and plastic sheets were removed. After at least 7 days of curing at room temperature, the single unit of liner was obtained and cut into four identical specimens using a diamond-bladed saw. A measuring tape was used to measure the outer diameter and width, and a digital caliper was used to measure the wall thickness of each specimen at eight different locations. The average dimensions are presented in Table 1.

### **Test Set-up and Instrumentation**

For testing the liner specimens, a customized parallel-plate compression loading test setup was prepared according to ASTM D2412 (2021) as shown in Figure 1. Each liner specimen was placed between two parallel plates with the size of 450 mm x 750 mm and the thickness of 12.7 mm. The bottom plate seated on the bottom beam of a self-reaction frame, while the top plated was connected to a hydraulic jack hanging from the top of the frame. A load cell was placed between

the top plate and the jack. The maximum stroke of the jack was 340 mm allowing large deformations with a displacement rate of 20 mm/min being applied to each specimen. For each specimen, four strain gauges were applied at the mid-section: one at crown, one at invert, one at each the springline positions as shown in Figure 1. All four strain gauges were applied at the tension sides. It means, the strain gauges at the springlines were applied on the exterior side of the liner and the strain gauges at crown/invert were applied on the interior side of the liner. All strain gauges were placed parallel to the fiber direction (i.e., the hoop direction).

As shown in Figure 1, to obtain the vertical and horizontal diametrical deformations, four displacement gauges known as string potentiometers were installed on each specimen. Two vertical string potentiometers were installed between the parallel plates (one at the front and one at the back of each specimen) to obtain vertical diametrical deformation in the direction of the load. Also, two horizontal string potentiometers were installed at the mid-height level of the specimen connecting the springline points (one at the front and one at the back) to obtain horizontal diametrical deformation in the direction perpendicular to the load. All the specimens were then tested under compressive transverse loading. Displacements in vertical and horizontal directions and strains at the springline and crown/invert positions were collected using a digital data acquisition system with a frequency of 10 Hz and were further processed.

## **EXPERIMENTAL RESULTS AND DISCUSSION**

In this section, the failure modes, the load-diametrical deformation behavior, and load-strain behavior of the test specimens are discussed. A summary of the results is presented in Table 2. Also, the overall pipe stiffness and the flexural rigidity of the specimens, which were obtained at two different level (i.e., 5% and 10%) of the vertical diametrical deflection are evaluated. A summary of the results is presented in Table 3. The details are discussed in the following sections.

## **Failure Modes**

The failure of the liners can be categorized into two main modes of (i) FRP failure and (ii) core failure as shown in Figure 2. The failure mode that the solid-wall liners experienced was the crushing of FRP at the inner face of the liner at the springline, which was followed by tensile rupture of FRP at the outer face of springline or crushing of FRP at the crown/invert. Sometimes, the delamination of the liner at the overlap area was also observed as the failure was progressed. For cases with intact fibers in the tension sides, the solid-wall liners were almost returned to their original shape and size after unloading due to elastic behavior of the fibers as shown in Figure 2(a). The sandwich liners, it was observed that the core shear was dominant at the shoulder and haunch positions of the liner and followed by delamination of the core from facesheet as shown in Figure 2(b). The shear failure was typically followed by crushing of the facesheets at the springlines and crown/invert. Overall, the sandwich liners showed higher stiffness when compared to solid-wall liners, however the strength of the sandwich liners was not more than the strength of their solid-wall counterpart due to the shear failure of the core, which is typical for sandwich structures with strong facesheets and weak core.

## **Load – Diametrical Deformation Behavior**

The experimental load vs. diametrical deformation curves of the specimens are presented in Figures 3-5. In the figures, the right side of the diagrams shows the vertical diameter changes, and the left side of the diagrams shows the horizontal diameter changes. The diameter changes were obtained using two parallel string potentiometers in each direction. The outcome of two parallel sensors were very close to each other and the average of the two measurements are presented in the diagrams.

Figure 3 presents the results of solid-wall specimens. It is evident that until an average load of 8 kN and 11 kN, the GFRP and CFRP specimens behave linearly, after which they start behaving non-linearly until they reach their peak load. This non-linearity is related to the geometric configuration of the system rather than the material properties. As the load increases, the circular liner starts becoming elliptical thereby recording large deflections and causing the specimen to behave non-linearly. This behavior is called elliptical ring deflection and the type of non-linearity caused is called geometric non-linearity. As expected, the CFRP specimens had a higher initial stiffness and peak load, hence showing minimum deflection when compared to GFRP specimens.

Figure 4 shows the results of the load vs. diametrical deflection response of GFRP and CFRP sandwich liners with the 3D woven fabric. It is noticeable that until a load of 7 kN and 9.5 kN, the GFRP and CFRP specimens tend to behave linearly after which they become non-linear. This non-linearity indicates the shearing of the core and simultaneous elliptical deformation that occurs when the specimens are being loaded. In general, for all the specimens with the 3D core, the core shear was the governing mode of failure.

Figure 5 presents the load vs. diametrical deflection behavior of GFRP and CFRP sandwich liners with the bulkermat core. It can be observed that the relation between load and diametrical deflection is linear for sandwich specimens with this core until it reaches its ultimate load capacity. It also shows that this composite has higher initial stiffness when compared to the solid-wall and 3D core sandwich specimens. While comparing the GFRP and CFRP specimens with the 3D core in terms of strength and stiffness, there is no significant difference. But a significant difference can be found between GFRP and CFRP specimens with bulkermat core where CFRP is stiffer and has a higher strength than GFRP sandwich specimens.

Overall, as shown in the figures and Table 2, the sandwich specimens with the bulkermat core had the highest peak load and stiffness. The sandwich specimens with the 3D woven fabric core had a comparable stiffness to the ones with the bulkermat core, but the 3D woven core was not strong enough and started to yield in shear.

### **Load – Strain Behavior**

Strains at the tension side of the springline and crown/invert positions of the specimens were also collected. Load vs. strain behavior of solid-wall GFRP and CFRP specimens are presented in Figure 6. Due to the loss of some strain gauges during the test, the curves indicating load – strain response were continued with slopes based on their previous slope until the failure load. It is evident that CFRP specimens show less strain under their corresponding peak loads when compared to GFRP specimens accounting for the higher stiffness in CFRP and higher flexibility in GFRP liners. Since the specimens undergo higher deflection in the vertical direction when compared to the horizontal direction, it is noticeable that the strain for a given load is higher at the crown/invert than the springline.

Load vs. strain behavior of the sandwich liners with 3D core are presented in Figure 7 based on strain data collected from the crown/invert and springline positions of the liner at the tension sides. The difference in strains for GFRP and CFRP sandwich liners at both springline and crown/invert positions are minimal. Like the solid-wall specimens, the strain at the crown/invert is higher than that at the springline, attributed to the greater vertical deflection relative to horizontal deflection. It can be noticed that the load vs. strain curves of the 3D core sandwich specimens are mostly non-linear due to the early yielding of the core in shear.

Load vs. strain curves of the sandwich liners with the bulkermat core are given in Figure 8. It is noticeable that the behavior is linear at both springline and crown/invert positions. As

expected, CFRP sandwiches has less strain due to its higher stiffness. Overall, the sandwich specimens with the bulkermat core likely exhibited a full-composite action unlike the sandwich specimens with the 3D core which likely exhibited a partial-composite due to the shear non-linearity of the core. This behavior was previously observed by testing flat sandwich specimens with the 3D woven core (McCracken and Sadeghian 2018b) and the bulkermat core (MacDonnell and Sadeghian 2020).

### **Pipe Stiffness and Stiffness Factor**

To evaluate the rigidity of the liners, two parameters of pipe stiffness and stiffness factor are calculated for each specimen per ASTM D2412 (2021). Pipe stiffness refers to the ability of a pipe to resist deformation under external loads, which is an important property in the design and analysis of underground or buried pipes. The ratio of force per unit length of a pipe ( $F$ ) to the vertical deflection ( $\Delta y$ ) is defined as pipe stiffness ( $PS$ ) as follows.

$$PS = F/\Delta y \quad (1)$$

Pipe stiffness is also the slope of the load vs. vertical diametrical deformation curve. The pipe stiffness at a vertical deflection equal to 5% of the average inside diameter of the specimen is typically used for design purposes and classification of pipes. On the other hand, as shown in Eq. (2), stiffness factor ( $SF$ ) is the product of pipe stiffness ( $PS$ ) and the quantity  $0.149r^3$ , which is derived using mechanics relating to the total strain energy stored in a ring specimen (ASTM D2412 2021).

$$SF = PS \times (0.149 r^3) \quad (2)$$

In fact, the stiffness factor ( $SF$ ) is equivalent to the flexural rigidity ( $EI$ ) of a pipe, which is a function of the material's flexural modulus ( $E$ ) and the moment of inertia ( $I$ ) of the wall of the pipe. However, the quantities pipe stiffness ( $PS$ ) and stiffness factor ( $SF$ ) are computed values

determined from the test resistance at a particular deflection. These values are highly influenced by the degree of deflection, as the radius changes with pipe deflection. The greater the deflection at which *PS* or *SF* are determined, the greater the magnitude of the deviation from the true *EI* value (ASTM D2412 2021).

In this study, the pipe stiffness and stiffness factor for all the specimens were calculated at both 2.5% and 5% vertical deflection and averaged as shown in Table 3. For the CFRP specimens with bulkermat core, no data is available for the 5% vertical deflection as the specimens did not reach that level. The results indicate that the pipe stiffness at 2.5% of the solid-wall GFRP specimens is 0.27 kN/mm/mm. By adding the 3D and bulkermat cores, the pipe stiffness increased to 1.04 and 1.72 kN/mm/mm, respectively (3.9 and 6.4 times, respectively). On the other hand, the pipe stiffness at 2.5% of the solid-wall CFRP specimens is 1.18 kN/mm/mm. By adding the 3D and bulkermat cores, the pipe stiffness decreased to 0.91 and increased to 3.64 kN/mm/mm, respectively (0.8 and 3.1 times, respectively). This indicates that the 3D core did not have enough shear rigidity for the CFRP facesheets. In addition, the bulkermat core was more effective on GFRP specimens than the CFRP ones.

The theoretical flexural rigidity (*EI*) of the wall of the test specimens was calculated using conventional cross-sectional analysis of the solid-wall and sandwich sections as follows.

$$EI = E_c \frac{wc^3}{12} + E_f \frac{wt_f^3}{6} + E_f \frac{wt_f d^2}{2} \quad (3)$$

The cross-sectional detail of a sandwich specimen is given in Figure 9. The *EI* for solid-wall specimens is based on the results from tensile coupon test. Ply thickness of the coupon was used to find the normalized elastic modulus and the second moment of area was calculated based on the section properties. The flexural rigidity was calculated per unit width and provided Table 3 for comparison with the stiffness factor. It can be observed that the stiffness factors of solid-wall

specimens are close to the corresponding  $EI$  values. However, that is not the case for sandwich specimens, which is likely due to the shear deformations of the core in the sandwich specimens, specially for the 3D core sandwich specimens with high non-linearity of the core in shear.

Overall, the 3D core did not have enough shear strength and stiffness to provide composite action between the FRP facesheets. The shortcoming was more evident in the specimens with CFRP facesheets due to higher demand of CFRP facesheets than GFRP facesheets. However, the bulkermat core did not have the issue. As CFRPs are stiffer than GFRPs, the bulkermat core showed higher stiffness for the sandwich specimens with CFRP facesheets.

In the following, an analytical model is developed to predict the test data based on the geometrical non-linearity the specimens. As the material non-linearity is not included, the model is not applicable to the sandwich specimens with the 3D core.

## **ANALYTICAL STUDIES**

### **Model Description**

During the parallel plate testing described in the experimental section, it was observed that a circular ring starts becoming elliptical, which create a geometrical non-linearity. Therefore, an analytical model was developed to predict the vertical and horizontal deflections using an iterative procedure. A code was written in Mathcad software to perform this iteration. The liner specimen was considered as a two-dimensional elliptical ring section, subjected to concentrated compressive forces along its vertical diameter. Due to symmetry, only a quadrant of the ring was considered for the analysis. Free body diagram of the elliptical ring with bending moments and the local constraints are shown in Figure 10. The magnitude of bending moment  $M_A$  in this cross-section was statically indeterminate and was found using Castigliano's theorem. Since there was no rotation at point A while bending, displacement corresponding to  $M_A$  was zero as follows:

$$dU/dM_A = 0 \quad (4)$$

where  $U$  is the strain energy of the quadrant of the ring. For any cross-section OX which is at an angle  $\theta$  with the horizontal the bending moment is given as,

$$M_1 = M_A - F/2 \rho \cos \theta \quad (5)$$

where,  $\rho$  is the radius of the curvature of the ellipse.

$$\rho = \frac{a \cdot b}{\sqrt{b^2 \cos^2 \theta + a^2 \sin^2 \theta}} \quad (6)$$

The decrease in vertical diameter was calculated based on Castigliano's theorem, using the total strain energy stored in the ring.

$$U = \frac{2}{EI} \int_0^{\pi/2} M_1^2 \rho d\theta \quad (7)$$

The vertical deflection  $\delta V$  was derived from the equation below:

$$\delta V = K_1 (F/EI) \quad (8)$$

where  $K_1$  is an integral obtained by differentiating the strain energy  $U$  with respect to  $M_A$  as given below,

$$K_1 = \int_0^{\pi/2} \left( \rho \cos \theta - \frac{\int_0^{\pi/2} \rho^2 \cos \theta d\theta}{\int_0^{\pi/2} \rho d\theta} \right) \rho^2 \cos \theta d\theta \quad (9)$$

To determine the horizontal deflection  $\delta_H$ , two equal and opposite imaginary forces  $Q$  were applied along the end of horizontal diameter. Calculating  $(dU/dQ)$  at  $Q = 0$  would give the horizontal deflection. Figure 10 shows the free body diagram to find the increase in horizontal deflection.

The moment  $M_2$  and  $M_1$  were summed up to find the  $\delta H$  as given below:

$$M_2 = M_B + Q/2 \rho \sin \theta \quad (10)$$

$$\delta H = K_2 (F/EI) \quad (11)$$

where  $K_2$  is an integral obtained by differentiating the strain energy  $U$  with respect to  $M_B$  as given below,

$$K_2 = \int_0^{\pi/2} \left( \frac{\int_0^{\pi/2} \rho^2 \cos\theta \, d\theta}{\int_0^{\pi/2} \rho \, d\theta} - \rho \cos\theta \right) \left( \rho \sin\theta - \frac{\int_0^{\pi/2} \rho^2 \sin\theta \, d\theta}{\int_0^{\pi/2} \rho \, d\theta} \right) \rho \, d\theta \quad (12)$$

For a sandwich specimen, the diametrical deflections were calculated based on the bending and shear. Thin facesheets resist the compressive and tensile stresses due to bending and the core material resists the shear. To calculate the decrease in vertical diameter, the analysis involved determining both the strain energy due to bending and shear. Strain energy due to bending was found as follows:

$$U_b = 4. \int_0^{\pi/2} M_1^2 \cdot \frac{\rho}{2.EI} \, d\theta \quad (13)$$

Strain energy due to shear was also found as follows:

$$U_s = 4. \int_0^{\pi/2} V^2 \cdot \frac{\rho}{2.G.A} \, d\theta \quad (14)$$

where  $V$  is the shear force and  $G$  is the shear modulus. The overall strain energy was taken as the sum of strain energy due to bending and strain energy due to shear. The vertical deflection was obtained from the equation below.

$$\delta V_{sandwich} = dU/dF \quad (15)$$

Similarly, the horizontal deflection was found using the strain energy due to bending and strain energy due to shear as functions of the load  $F$  and imaginary forces  $Q$ . The horizontal deflection was determined using the equation below.

$$\delta H_{sandwich} = dU/dQ \quad (16)$$

## **Geometrical Nonlinearity**

This analytical model was generated by considering the geometric nonlinearity that the liners exhibit while being loaded, through an iterative procedure. Under transverse compression, the circular liner starts failing elliptically with a decrease in vertical diameter and increase in horizontal diameter. The significant change of the geometric properties causes a large deformation which makes the load – diametrical deflection and load – strain behavior of the liner non-linear. This is because the stiffness of the liner changes with the deformation of shape of liner, causing a type of non-linearity called geometric non-linearity. To mimic this ellipticity, a load of 500 N was added to the circular liner initially.  $\delta V$  and  $\delta H$  were calculated under this load and added to the initial diameters respectively and a new radius of curvature was determined. Corresponding strains at springline and crown/invert positions were found simultaneously. For further iterations, the liner with the new radius of curvature were loaded with a force of 500 N consecutively, until the iterative data up to the desired load is obtained. Based on the data obtained from the iterations, load – diametrical deflection and load – strain curves are plot. A flowchart of this entire process is presented in Figure 11.

## **Model Verification**

Figure 12 shows the verification of the analytical model against load vs. diametrical deflection behavior of the solid-wall and bulkermat core sandwich specimens. The 3D woven core sandwich specimens are not included as the model is not able to predict the material non-linearity of the core. From Figure 12(a) it is evident that the model fits the data very well. GFRP being a flexible material deflects significantly under load and thereby shows large levels of deflections when compared to CFRP. These high levels of deflection in GFRP after an average load of 3kN causes geometric non-linearity in the solid-wall specimen's behavior. The model can capture the

geometric non-linearity that the solid-wall GFRP specimens display prominently while sufficiently accommodating the linear behavior that the solid-wall CFRP specimens show. The model can validate that the GFRP specimens have a low stiffness until an average load of 9 kN and then starts gaining until it ultimately fails due to geometric non-linearity.

Figure 12(b) shows the model verification against the test results of load vs. deflection the sandwich specimens with the bulkermat core. The model can predict the behavior of the bulkermat core sandwich specimens with GFRP facesheet very well, however for the specimens with CFRP facesheets there is test data shows more nonlinearity than the model at higher load levels. This is likely because the high stiffness of the CFRP facesheets generated high shear stress in the core beyond its linear behavior, which is not included in the model.

Figure 13 shows the verification of the analytical model against the load vs. strain behavior of the specimens. As it was mentioned in the experimental program, during the test some strain gauges were lost at high strain levels and corresponding curves were continued up to the average peak load based on their previous slopes as shown with dotted lines in the figures. It is evident that the model can predict the behavior of all solid-wall specimens plus the bulkermat core sandwich specimens with GFRP facesheets. Similar to load-deflection behavior, for the bulkermat core sandwich specimens with CFRP facesheets, the model is stiffer than the test, which is likely due to the fact that the model was developed to accommodate only geometric non-linearity, not material non-linearity as it was mentioned earlier.

Overall, the analytical model predicts the behavior of all solid-wall specimens considering the geometric non-linearity of flexible GFRP specimens. For sandwich specimens, as long as the core material does not yield in shear, the model is able to predict their behavior. For future studies, the analytical model needs to be advanced to include the material non-linearity of cores in shear.

## Parametric Study

A parametric study was conducted to study the effect of liner diameter, facesheet thickness, core thickness of the bulkermat sandwich liners and the shape geometry. The parameters held constant while investigating the effect of the main parameter included liner width  $W$  at 300 mm, facesheet elastic modulus  $E_f$  at 21.75 GPa, facesheet thickness  $t_f$  at 1.3 mm/ply, core thickness  $c$  at 1.24 mm, core elastic modulus  $E_c$  at 374 MPa, and core shear strength  $\tau_{max}$  at 2.2 MPa. Figure 9 shows the geometrical parameters on a given section of sandwich wall. The mechanical properties were selected based on the information presented in Section “Material Properties”. The results of the parametric study are briefly reported in Table 4.

***Effect of Liner Diameter:*** Three diameters of 300, 600, and 900 mm were considered for sold-wall liners with 4 layers of GFRP. The outcome of the analysis is shown in Table 4. As the diameter increases, the peak load of the liner decreases. For example, by increasing the diameter from 300 to 900 mm, the strength of the liner reduces by 67.2%. As expected, the stiffness factor does not change significantly.

***Effect of Core Thickness:*** The bulkermat core was added to the 4-layer GFRP liners with the diameter of 600 mm. Three core thicknesses of 4, 8, and 12 mm were considered. As shown in Table 4, both the peak strength and stiffness factor increase as the core thickness increases. For example, when the core thickness is increased from 0 to 12 mm, the peak load increases by 66%. Based on Table 4, it is seen that the stiffness factor at 2.5% and 5% vertical deflection increases as the core thickness increases. For example, there is an increase in stiffness by 95.72% at 2.5% when the core thickness is increased from zero to 12 mm. Geometric non-linearity becomes less prominent with the increase in stiffness of the liners. Core shear was the governing failure mode for all sandwich liners.

***Effect of Facesheet Thickness:*** The facesheet thickness was varied between 1 to 3 layers with one layer being 1.3 mm thick. As shown in Table 4, the strength and stiffness increase with an increase in facesheet thickness. For example, as the facesheet thickness increases from 1 to 3 layers, the strength increases by 55%. Although there is an increase in stiffness, the geometric non-linearity of the liners is slightly observable. The failure mode for all the specimens were core shear.

***Effect of Shape Geometry:*** The liner shape was varied from a circle to an ellipse with constant width ( $2a$ ) and variable height ( $2b$ ) as follows:  $2a = 2b = 600$  mm,  $2a = 600$  mm  $\times$   $2b = 450$  mm and  $2a = 600$  mm  $\times$   $2b = 300$  mm. The effect of shape geometry was studied for both solid-wall and bulkermat sandwich liners. Table 4 shows that by decreasing the height (changing circle to ellipse), the stiffness of both solid-wall and sandwich liners decreases, however the strength of solid-wall liners slightly increases and that of sandwich liners slightly decreases. For instance, for solid-wall liners, changing the height from 600 mm (Case #2) to 450 mm (Case #10) results in a decrease in the stiffness factor (at 2.5%) from 255 to 120, accompanied by an increase in the peak load from 8.0 kN to 9.2 kN. Conversely, for sandwich liners, altering the height from 600 mm (Case #4) to 450 mm (Case #11) leads to a reduction in the stiffness factor (at 2.5%) from 1219 to 573, alongside a decrease in the peak load from 14.5 kN to 14.2 kN. Generally, changing the liners from a circular to an elliptical shape (without altering the horizontal projection) enhances flexibility without a significant impact on strength.

## **CONCLUSIONS**

In this study, the performance of GFRP and CFRP solid-wall and sandwich liners with either 3D woven fabric core or bulkermat core under parallel-plate compression loading was evaluated. For solid-wall liners, crushing at springline was the governing mode of failure whereas for both sandwich liners, core shear was the governing failure. Large deformations were evident in the thin-

walled liners, especially in the solid-wall liners. Adding the cores was effective in increasing the stiffness and strength of the liners, however the 3D woven fabric core was not stiff and strong enough in shear to develop high degree of composite action between the facesheets of the sandwich system. On the other hand, the bulkermat core showed reasonable stiffness and strength transferring shear stresses between the facesheets. An iterative analytical model based on geometric non-linearity of the liners was developed to find elliptical ring deflections of the liners. The analytical model was in good agreement with the test results of the solid-wall and bulkermat sandwich liners, however the model was not able to predict the behavior of the 3D core sandwich liners due to material non-linearity of the 3D core in shear. A parametric study was also conducted to evaluate the effect of parameters such as liner diameter, bulkermat core thickness, facesheet thickness and shape geometry. Future works based on this research can include adding the material non-linearity to the analytical model and evaluating the behavior of the liners after bonding inside concrete culverts.

## **ACKNOWLEDGEMENT**

The support and assistance provided by the technicians (Jordan Maerz, Jesse Keane, and Brian Kennedy) in the Department of Civil and Resource Engineering at Dalhousie University for fabricating and testing the specimens is greatly appreciated. The authors would like to thank QuakeWrap Inc. (Tucson, AZ, USA) for providing all the materials that was used for this research.

## **DATA AVAILABILITY STATEMENT**

Some or all data, models, or code that support the findings of this study are available from the corresponding author upon reasonable request.

## REFERENCES

- Abraham, D. M., and Gillani, S. A. (1999). Innovations in materials for sewer system rehabilitation. *Tunnelling and Underground Space Technology*, 14(1), 43-56.
- Allen, H. G. (2013). *Analysis and design of structural sandwich panels*. Pergamon Press, Oxford, UK.
- Arjomandi, K., and Taheri, F. (2010). Elastic buckling capacity of bonded and unbonded sandwich pipes under external hydrostatic pressure. *Journal of Mechanics of Materials and Structures*, 5(3), 391-408.
- Arjomandi, K., and Taheri, F. (2011). A new look at the external pressure capacity of sandwich pipes. *Marine Structures*, 24(1), 23-42.
- Arjomandi, K., and Taheri, F. (2012). Bending capacity of sandwich pipes. *Ocean Engineering*, 48, 17-31.
- ASTM D2412-21. (2021). *Standard Test Method for Determination of External Loading Characteristics of Plastic Pipe by Parallel-Plate Loading*. American Society of Testing and Materials International, West Conshohocken, PA, USA.
- Aylor Jr, H. H., and Hirtz, B. A. (1990). Method of reconstructing pipe systems using fiberglass laminates. U.S. Patent No. 4,897,135, January 30, 1990.
- Betts, D., Sadeghian, P., and Fam, A. (2018). Experimental behavior and design-oriented analysis of sandwich beams with bio-based composite facings and foam cores. *Journal of Composites for Construction*, 22(4).
- Das, R. R., and Baishya, N. (2016). Failure analysis of bonded composite pipe joints subjected to internal pressure and axial loading. *Procedia Engineering*, 144, 1047-1054.

- Deniz, M. E., Ozen, M., Ozdemir, O., Karakuzu, R., and Icten, B. M. (2013). Environmental effect on fatigue life of glass–epoxy composite pipes subjected to impact loading. *Composites: Part B*, 44(1), 304-312.
- Ehsani, M. (2017). ASCE Innovation Award Winner: Sandwich Construction Carbon FRP Pipe. *Pipelines 2017*, Phoenix, Arizona, 10-25.
- Hansen, U. (1998). Compression behavior of FRP sandwich specimens with interface debonds. *Journal of Composite Materials*, 32(4), 335-360.
- Houssam, T., and Sean, D. (2001). Stress modeling of pipelines strengthened with advanced composites materials. *Thin-Walled Structures*, 39(2), 153-165.
- Imoto, T., Seshimo, M., Makimoto, F., Kitagawa, E., and Ashimori Industry Co Ltd. (1993). Lining material for pipelines and a process for providing pipe lines therewith. U.S. Patent 5,186,987, 1993.
- Jianghong, X., Yiou, W., and Ding, Y. (2015). A shear deformation theory for bending and buckling of undersea sandwich pipes. *Composite Structures*, 132, 633-643.
- Karbhari, V. M. (2015). *Rehabilitation of pipelines using fiber-reinforced polymer (FRP) composites*. Elsevier.
- Kittson, M., and Kulawic, S. (1998). Pressure-expandable conduit liner. U.S. Patent No. 5,836,357, November 17, 1998.
- Karbhari, V. M., and Seible, F. (2000). Fiber Reinforced composites–advanced materials for the renewal of civil infrastructure. *Applied Composite Materials*, 7, 95-124.
- Lee, D. C., and Karbhari, V. M. (2005). Rehabilitation of large diameter prestressed cylinder concrete pipe (PCCP) with FRP composites – Experimental investigation. *Advances in Structural Engineering*, 8(1), 31-44.

- Liu, H., Luo, B., and Li, L. (2017). Design and mechanical tests of FRP pipe with bamboo and veneer layer. *BioResources*, 12(2), 2699-2710.
- MacDonnell, L., and Sadeghian, P. (2020). Experimental and analytical behavior of sandwich composites with glass fiber-reinforced polymer facings and layered fiber mat cores. *Journal of Composite Materials*, 54(30), 4875-4887.
- McCracken, A., and Sadeghian, P. (2018a). Corrugated cardboard core sandwich beams with bio-based flax fiber composite skins. *Journal of Building Engineering*, 20, 114-122.
- McCracken, A., and Sadeghian, P. (2018b). Partial-composite behavior of sandwich beams composed of fiberglass facesheets and woven fabric core. *Thin-Walled Structures*, 131, 805-815.
- Parashar, A., and Mertiny, P. (2011). Impact of scaling on fracture strength of adhesively bonded fibre-reinforced polymer piping. *Procedia Engineering*, 10, 455-459.
- Park, J., Hong, W., Lee, W., Park, J., and Yoon, S. (2014). Pipe stiffness prediction of buried GFRP flexible pipe. *Polymers and Polymer Composites*, 22(1), 17-23.
- Rafiee, R., and Habibagahi, M. R. (2018a). Evaluating mechanical performance of GFRP pipes subjected to transverse loading. *Thin-Walled Structures*, 131, 347-359.
- Rafiee, R., and Habibagahi, M. R. (2018b). On the stiffness prediction of GFRP pipes subjected to transverse loading. *KSCE Journal of Civil Engineering*, 22(11), 4564-4572.
- Rafiee, R., and Elasm, F. (2017). Theoretical modeling of fatigue phenomenon in composites pipes. *Composite Structures*, 161, 256-263.
- Rafiee, R. (2016). On the mechanical performance of glass-fibre-reinforced thermosetting-resin pipes: A review. *Composite Structures*, 143, 151-164.

- Simpson, B., Hoult, N. A., and Moore, I. D. (2017). Rehabilitated reinforced concrete culvert performance under surface loading. *Tunnelling and Underground Space Technology*, 69, 52-63.
- Syachrani, S., Jeong, H. S. D., Rai, V., Chae, M. J., & Iseley, T. (2010). A risk management approach to safety assessment of trenchless technologies for culvert rehabilitation. *Tunnelling and Underground Space Technology*, 25(6), 681-688.
- Tarakcioglu, N., Samanci, A., Arikan, H., and Akdemir, A. (2007). The fatigue behavior of  $(\pm 55^\circ)_3$  filament wound GRP pipes with a surface crack under internal pressure. *Composite Structures*, 80(2), 207-211.
- Wakayama, S., Kobayashi, S., Kiuchi, N., Sohda, Y., and Matsumoto, T. (2002). Improvement of the burst strength of FW-FRP composite pipes after impact using low-modulus amorphous carbon fiber. *Advanced Composite Materials*, 11(3), 319-330.
- Walsh, T. (2011). The plastic piping industry in North America. In *Applied Plastics Engineering Handbook* (pp. 585-602). William Andrew Publishing.
- Wang, Z., Chen, Z., He, Y., and Liu, H. (2017). Numerical study on lateral buckling of fully bonded sandwich pipes. *International Journal of Steel Structures*, 17(3), 863-875.
- Wang, Z., Ma, X., Liu, Y., Hui, M. A., and Guo, H. (2016). The mechanical behaviour and failure mode of FRP composite steel casing joints. *Polymers and Polymer Composites*, 24(2), 91-97.
- Zhao, J. Q., and Rajani, B. (2002). Construction and rehabilitation costs for buried pipe with a focus on trenchless technologies. Ottawa: NRC, Institute for Research in Construction.
- Zinno, A., Fusco, E., Prota, A., and Manfredi, G. (2010). Multiscale approach for the design of composite sandwich structures for train application. *Composite Structures*, 92, 2208–2219.

**Table 1: Test matrix**

<b>Group #</b>	<b>Specimen group ID</b>	<b>Specimen type</b>	<b>FRP type</b>	<b>Core type</b>	<b>Inner diameter (mm)</b>	<b>Width (mm)</b>	<b>Wall thickness (mm)</b>	<b>No. of identical specimens</b>
<b>1</b>	<b>4G</b>	Solid-wall	Glass	-	330	315	4.3	4
<b>2</b>	<b>4C</b>	Solid-wall	Carbon	-	335	316	5.3	4
<b>3</b>	<b>2G-W-2G</b>	Sandwich	Glass	3D Woven fabric	335	307	11.4	4
<b>4</b>	<b>2C-W-2C</b>	Sandwich	Carbon	3D Woven fabric	336	316	12.3	4
<b>5</b>	<b>2G-B-2G</b>	Sandwich	Glass	Bulkermat	335	304	9.6	4
<b>6</b>	<b>2C-B-2C</b>	Sandwich	Carbon	Bulkermat	335	303	9.9	4
<b>Total</b>								24

**Table 2: Summary of test results**

<b>Group #</b>	<b>Specimen Group ID</b>	<b>Peak Load (kN)</b>		<b>Vertical Deflection at Peak Load (mm)</b>		<b>Horizontal Deflection at Peak Load (mm)</b>		<b>Failure mode</b>
		<b>AVG</b>	<b>SD</b>	<b>AVG</b>	<b>SD</b>	<b>AVG</b>	<b>SD</b>	
<b>1</b>	<b>4G</b>	11.50	1.40	187.0	15.7	117.0	5.5	FRP Failure
<b>2</b>	<b>4C</b>	13.00	0.12	63.5	27.8	42.8	13.9	FRP Failure
<b>3</b>	<b>2G-W-2G</b>	10.60	0.93	194.0	44.9	119.5	22.8	Core Failure
<b>4</b>	<b>2C-W-2C</b>	11.50	0.61	152.0	30.5	90.9	14.8	Core Failure
<b>5</b>	<b>2G-B-2G</b>	13.07	1.54	59.0	54.0	37.0	29.0	Core Failure
<b>6</b>	<b>2C-B-2C</b>	13.15	1.64	18.0	12.0	12.0	6.0	Core Failure

Note: AVG = Average; and SD = Standard Deviation

**Table 3: Summary of experimental pipe stiffness and stiffness factor at 2.5 and 5% and theoretical flexural rigidity.**

Group #	Specimen Group ID	PS at 2.5% (kN/mm/mm)		PS at 5% (kN/mm/mm)		SF at 2.5% (kN-mm <sup>2</sup> /mm)		SF at 5% (kN-mm <sup>2</sup> /mm)		EI (kN-mm <sup>2</sup> /mm)
		AVG	SD	AVG	SD	AVG	SD	AVG	SD	Theoretical
<b>1</b>	<b>4G</b>	0.27	0.02	0.25	0.01	188	9	173	11	173
<b>2</b>	<b>4C</b>	1.18	0.02	1.14	0.04	878	8	849	24	1024
<b>3</b>	<b>2G-W-2G</b>	1.04	0.12	0.86	0.1	807	100	666	84	2265
<b>4</b>	<b>2C-W-2C</b>	0.91	0.05	0.79	0.06	705	33	614	33	10888
<b>5</b>	<b>2G-B-2G</b>	1.72	0.06	1.71	0.05	1225	53	1216	43	1422
<b>6</b>	<b>2C-B-2C</b>	3.64	0.61	NA	NA	2575	436	NA	NA	6416

Note: PS = pipe stiffness (see Eq. 1); and SF=stiffness factor (see Eq. 2); EI=theoretical flexural rigidity; NA=not available due to failure.

**Table 4: Summary of parametric study**

Case #	Outer Diameter <sup>1</sup> (mm)	Core Thickness <sup>2</sup> (mm)	FRP Layers <sup>3</sup>	Stiffness Factor <sup>4</sup> at 2.5%	Stiffness Factor <sup>4</sup> at 5%	Peak load (kN)	Vertical Def. at Peak Load (mm)	Mode of Failure
1	300	0	4	251	246	16.0	126.2	FRP Failure
2	600	0	4	255	221	8.0	505.0	FRP Failure
3	900	0	4	255	255	5.2	891.2	FRP Failure
4	600	4	2+2	1219	1194	14.5	180.3	Core Shear
5	600	8	2+2	2916	2861	18.5	86.6	Core Shear
6	600	12	2+2	5262	5167	23.5	57.8	Core Shear
7	600	4	1+1	398	389	9.2	386.5	Core Shear
8	600	4	2+2	1005	1091	14.2	179.4	Core Shear
9	600	4	3+3	1683	2115	20.5	115.8	Core Shear
10	600 × 450	0	4	120	120	9.2	392.1	FRP Failure
11	600 × 450	4	2+2	573	568	14.2	140.8	Core Shear
12	600 × 300	0	4	43	43	9.5	261.0	FRP Failure
13	600 × 300	4	2+2	200	120	14.2	105.1	Core Shear

Note 1: For elliptical shapes, the outer diameter is presented as width (horizontal) × height (vertical).

Note 2: The core thickness 0 means that the liner is a solid-wall liner.

Note 3: For sandwich liners, the figures 1+1, 2+2, or 3+3 indicate 1, 2, or 3 layers of FRP per skin. For solid-wall liners, the total number of FRP layers are presented.

Note 4: The unit of Stiffness Factor is kN-mm<sup>2</sup>/mm.

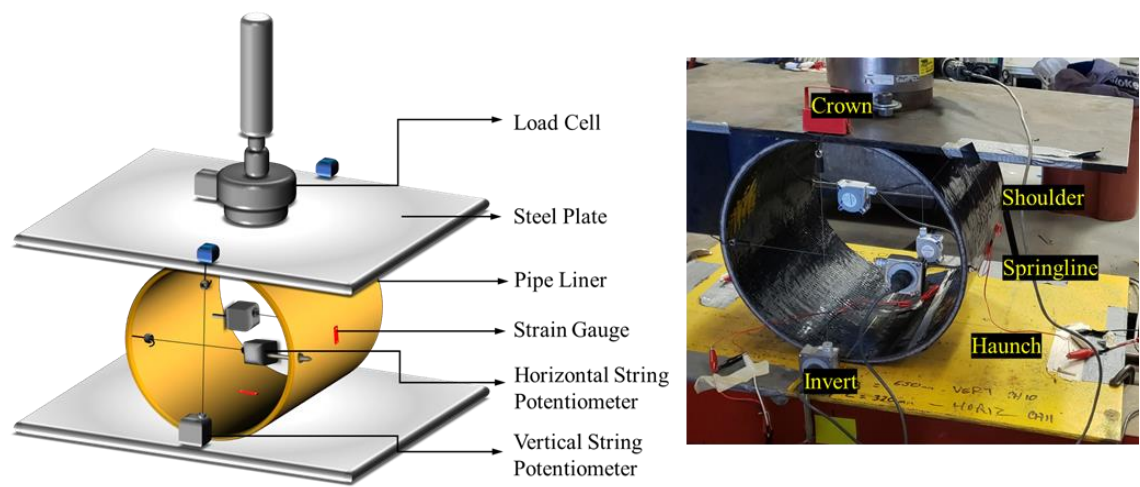
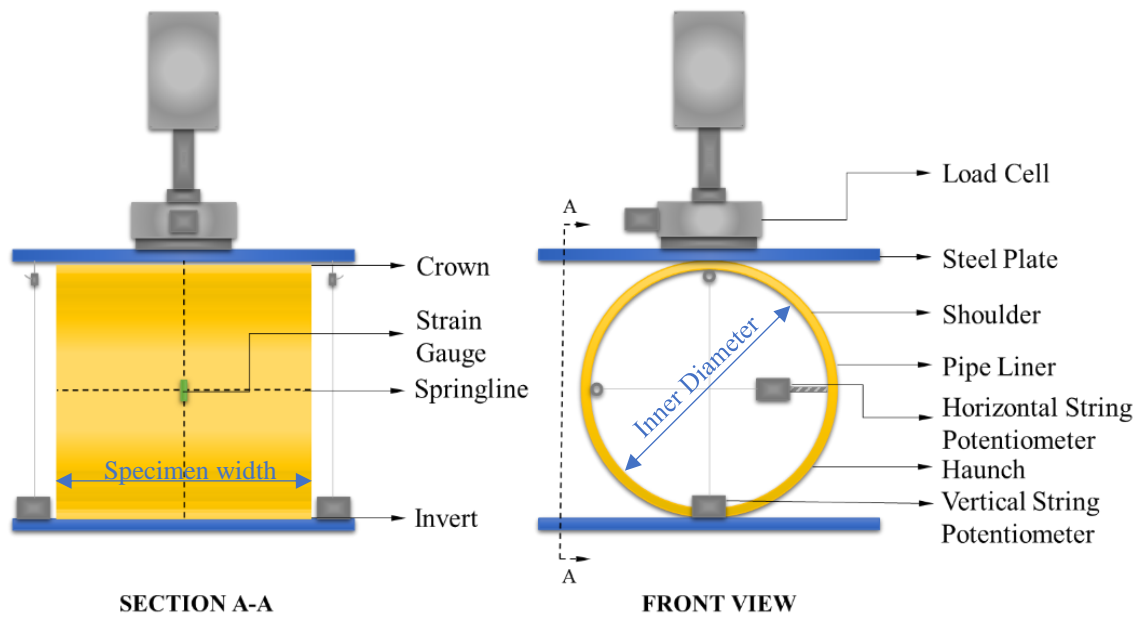


**Figure 1: Schematic drawings and photograph of test set-up and instrumentation**

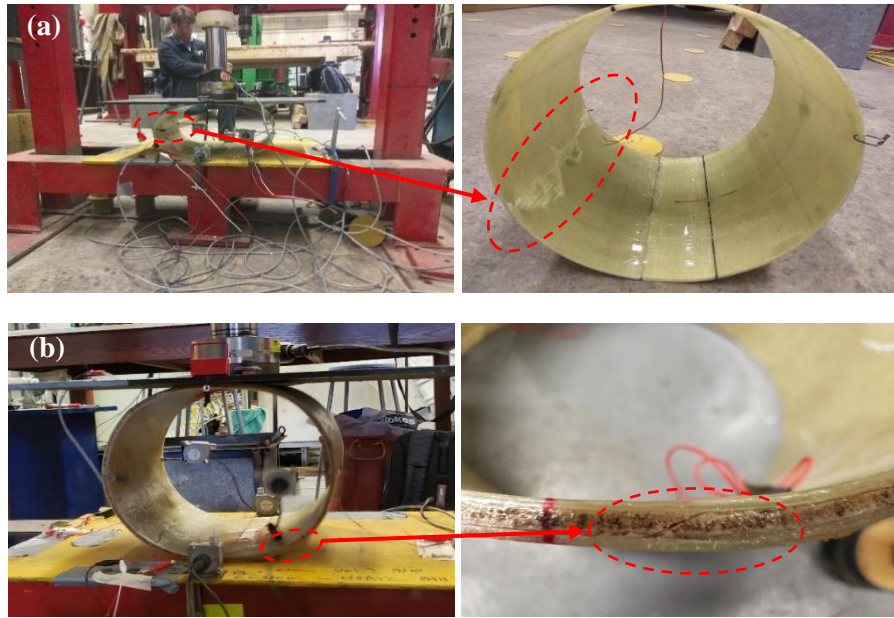


**Figure 2: Typical modes of failure: (a) FRP failure and (b) core failure.**

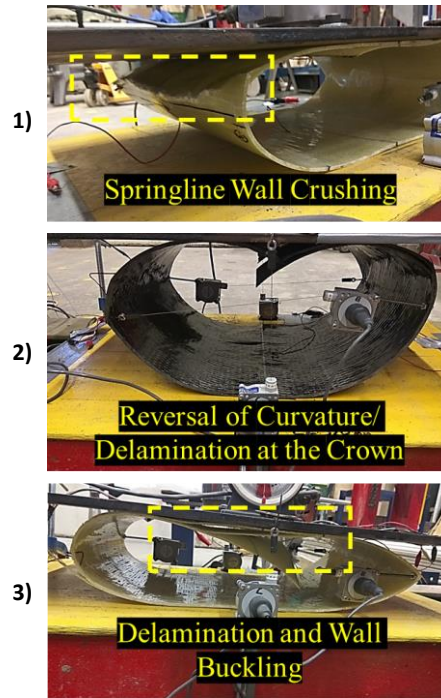
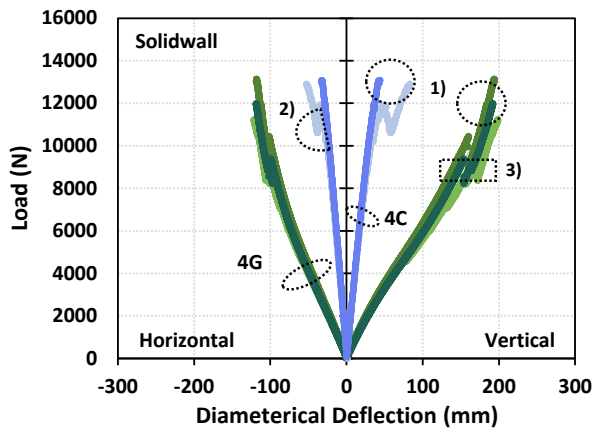


**Figure 3: Load vs. diametrical deflection behavior and failure of solid-wall specimens (4G and 4C) made of GFRP and CFRP.**

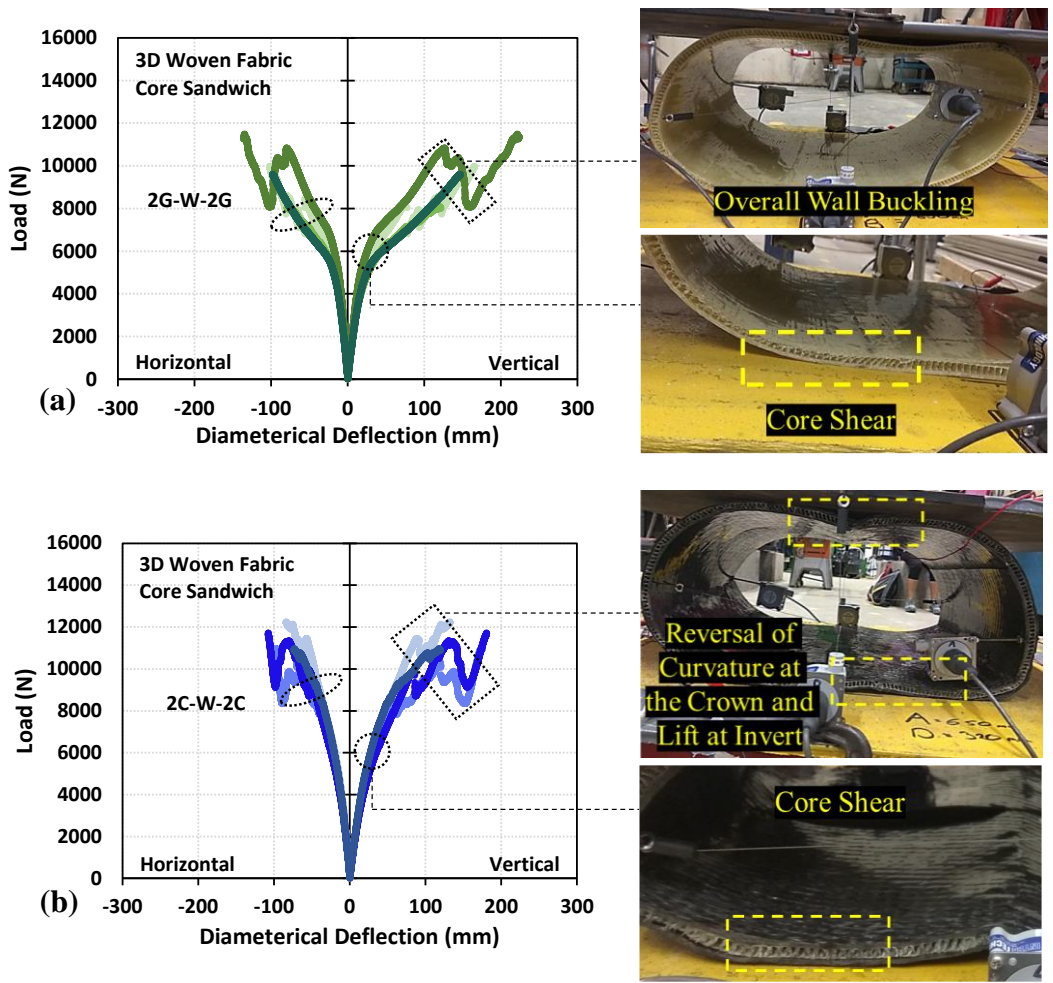
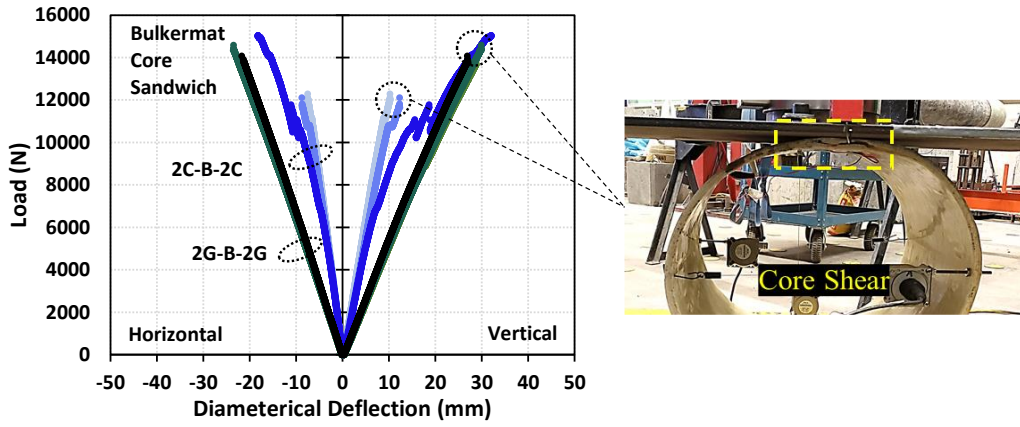
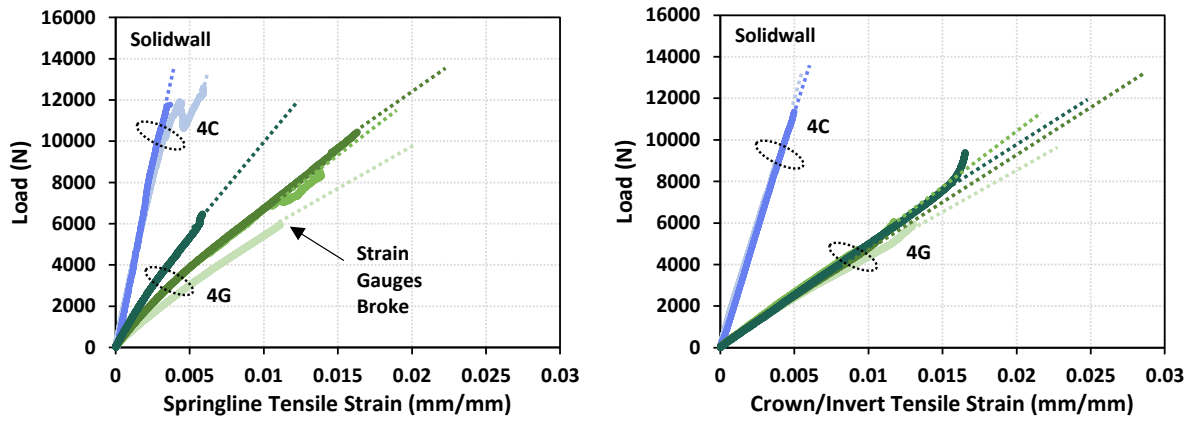


Figure 4: Load vs. diametrical deflection behavior and failure of sandwich specimens with 3D woven fabric core: (a) GFRP facesheets; and (b) CFRP facesheets.



**Figure 5: Load vs. diametrical deflection behavior and failure of sandwich specimens with bulkermat core.**



**Figure 6: Load vs. strain behavior of solid-wall specimens.**

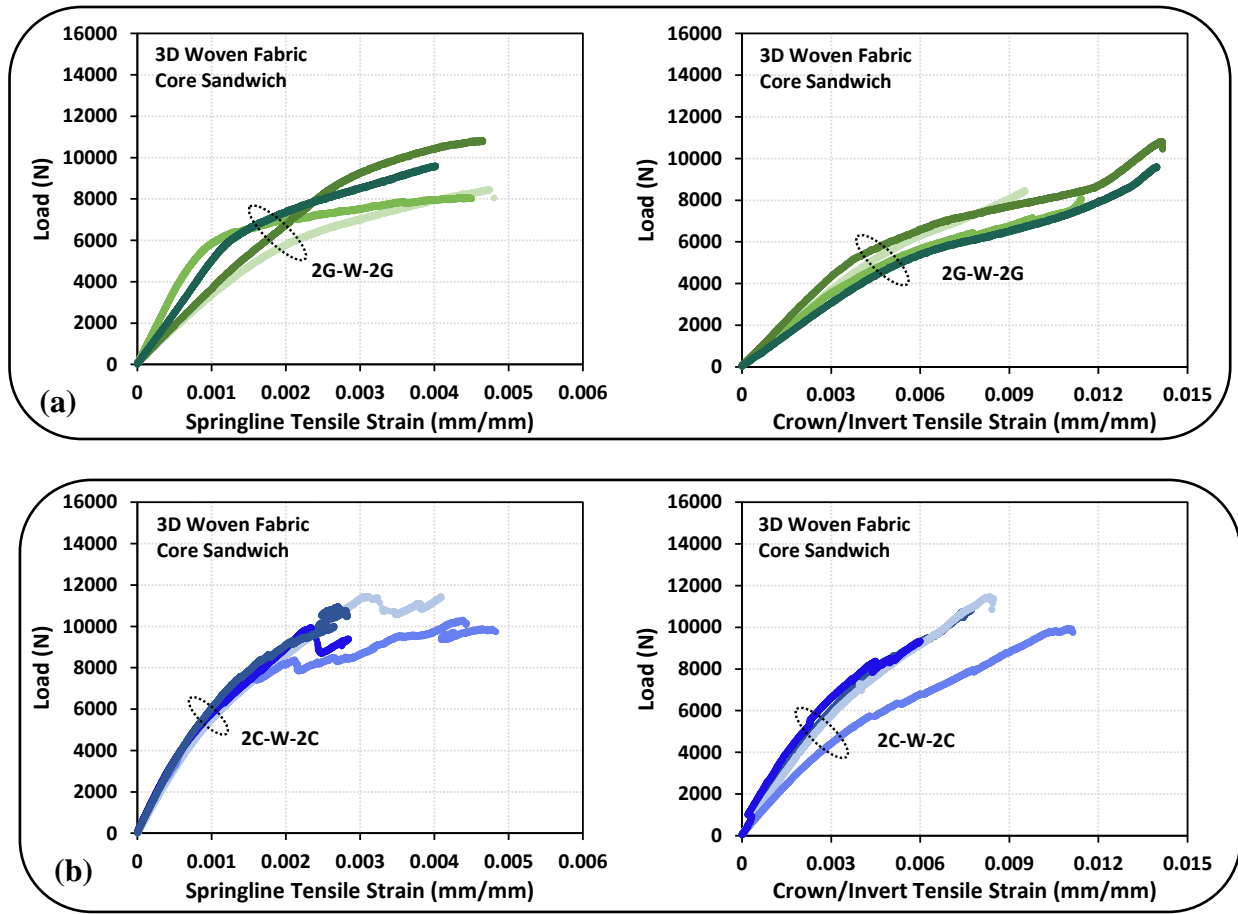


**Figure 7: Load vs. strain behavior of sandwich specimens with 3D woven fabric core: (a) GFRP facesheets; and (b) CFRP facesheets.**

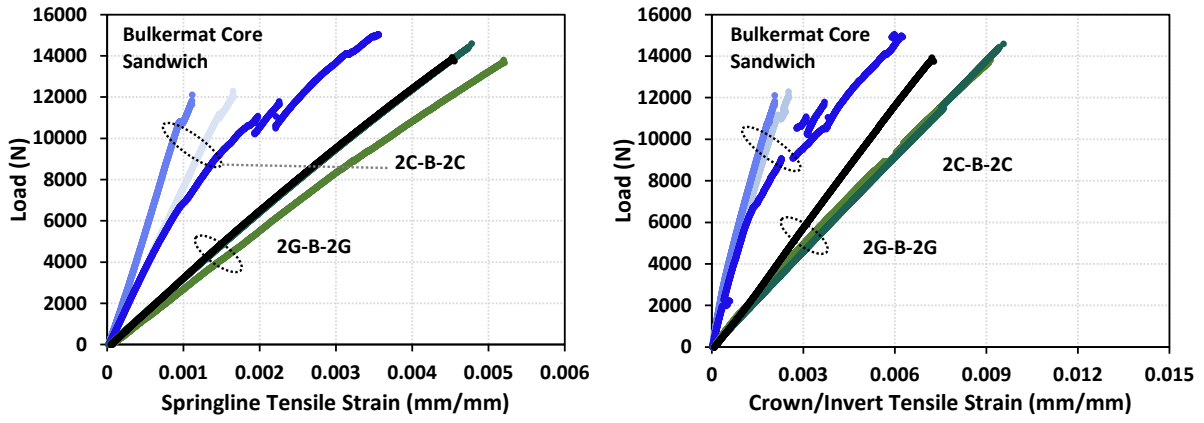


**Figure 8: Load vs. strain behavior of sandwich specimens with bulkermat core.**

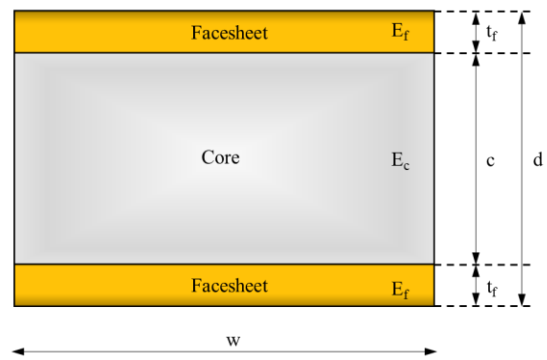


**Figure 9: Typical cross – section of a sandwich specimen**

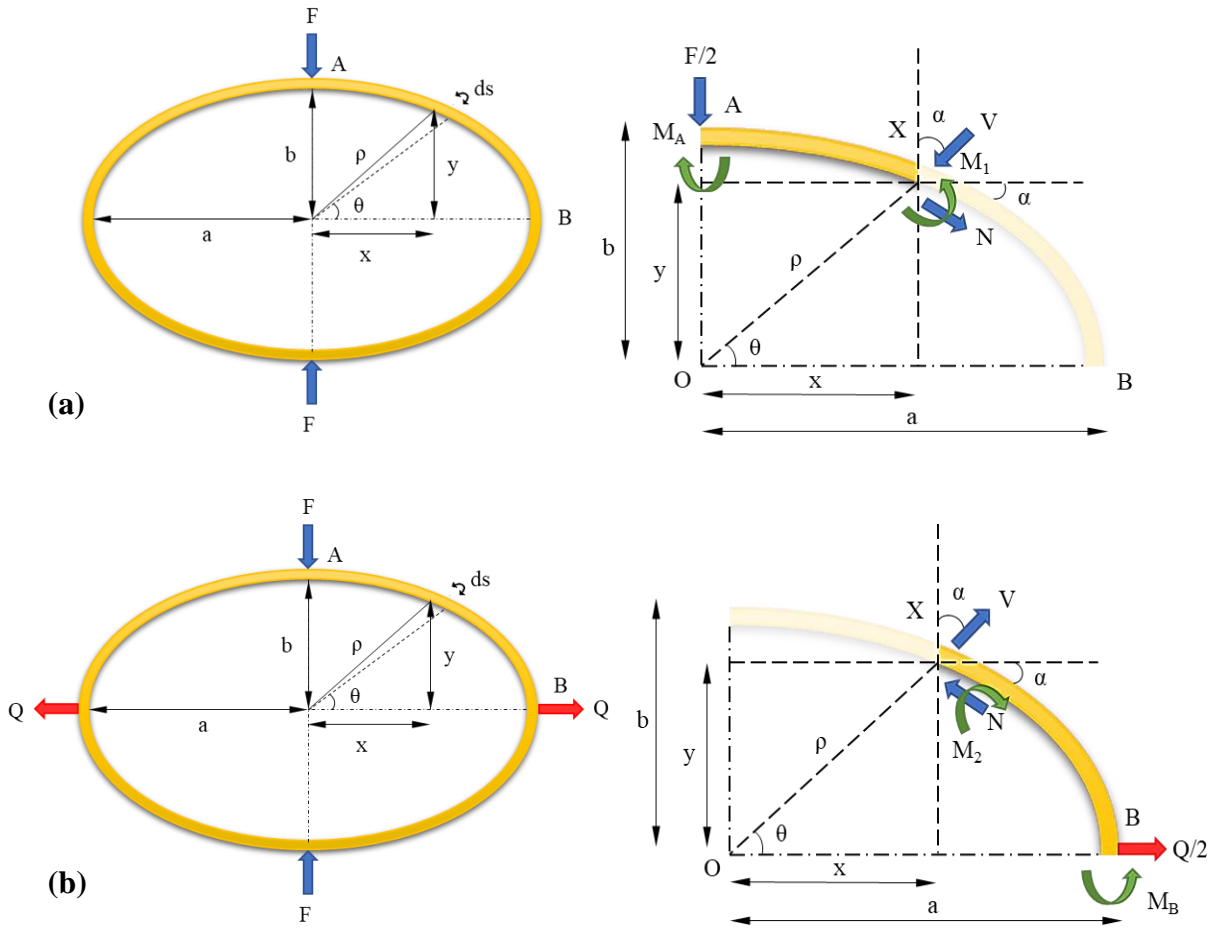


**Figure 10: Free body diagram of the elliptical ring to calculate (a) vertical and (b) horizontal deflection.**

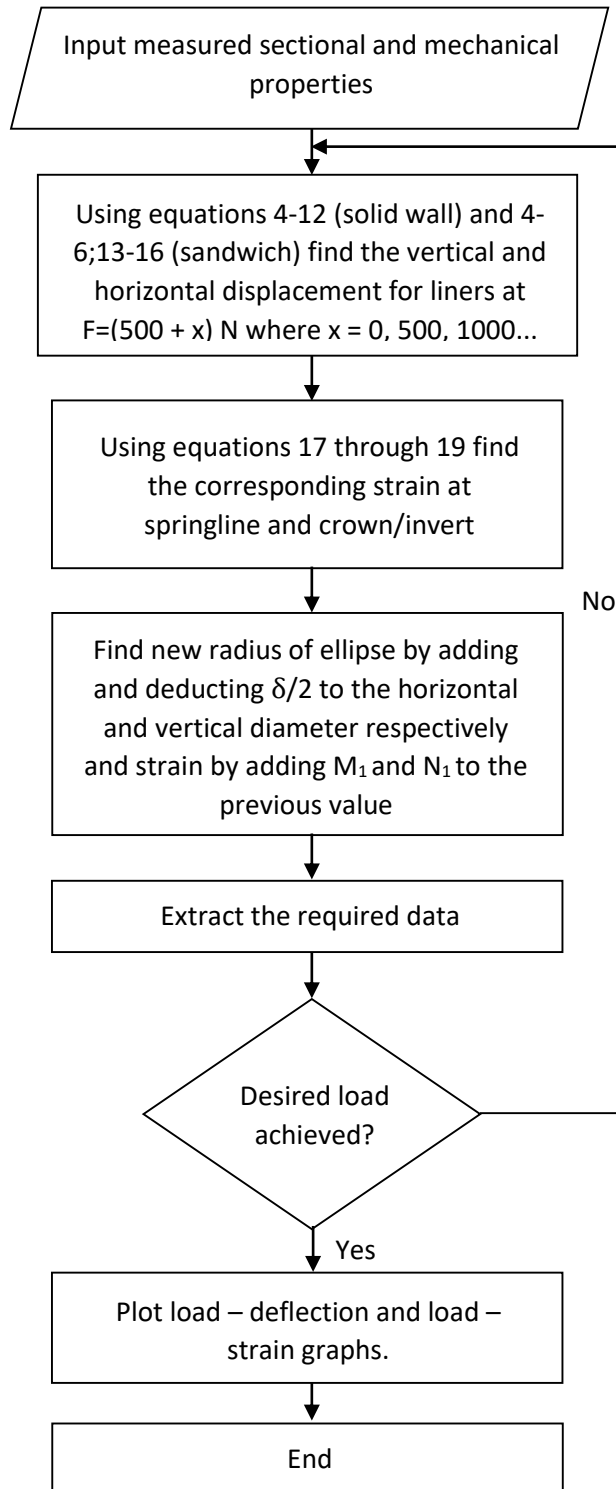


**Figure 11: Flowchart describing the steps of analytical modeling.**

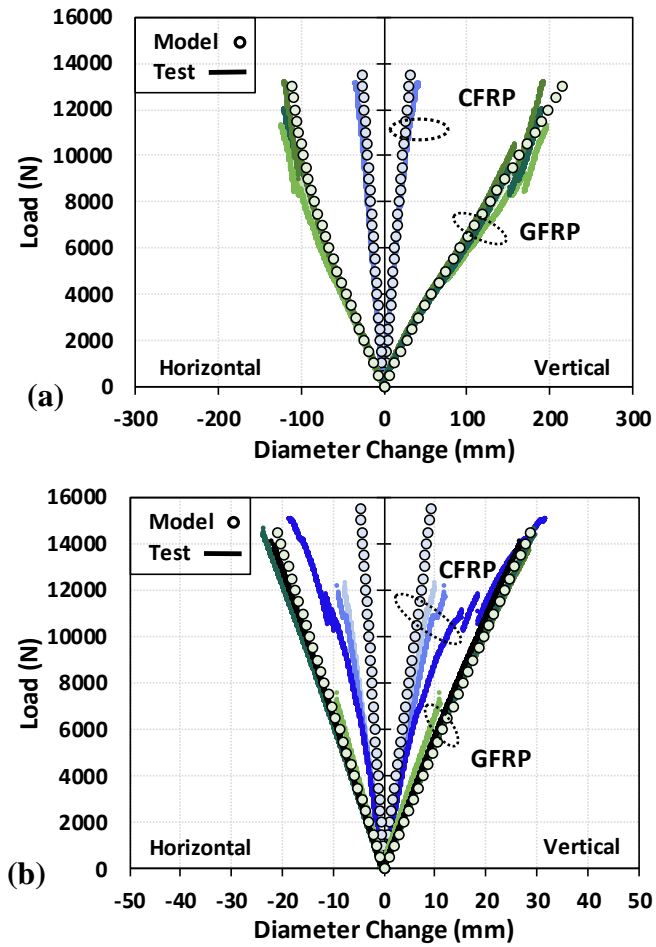


**Figure 12: Verification of analytical model based on load vs. diametrical deflection: (a) solid-wall specimens; and (b) sandwich specimens with bulkermat core.**

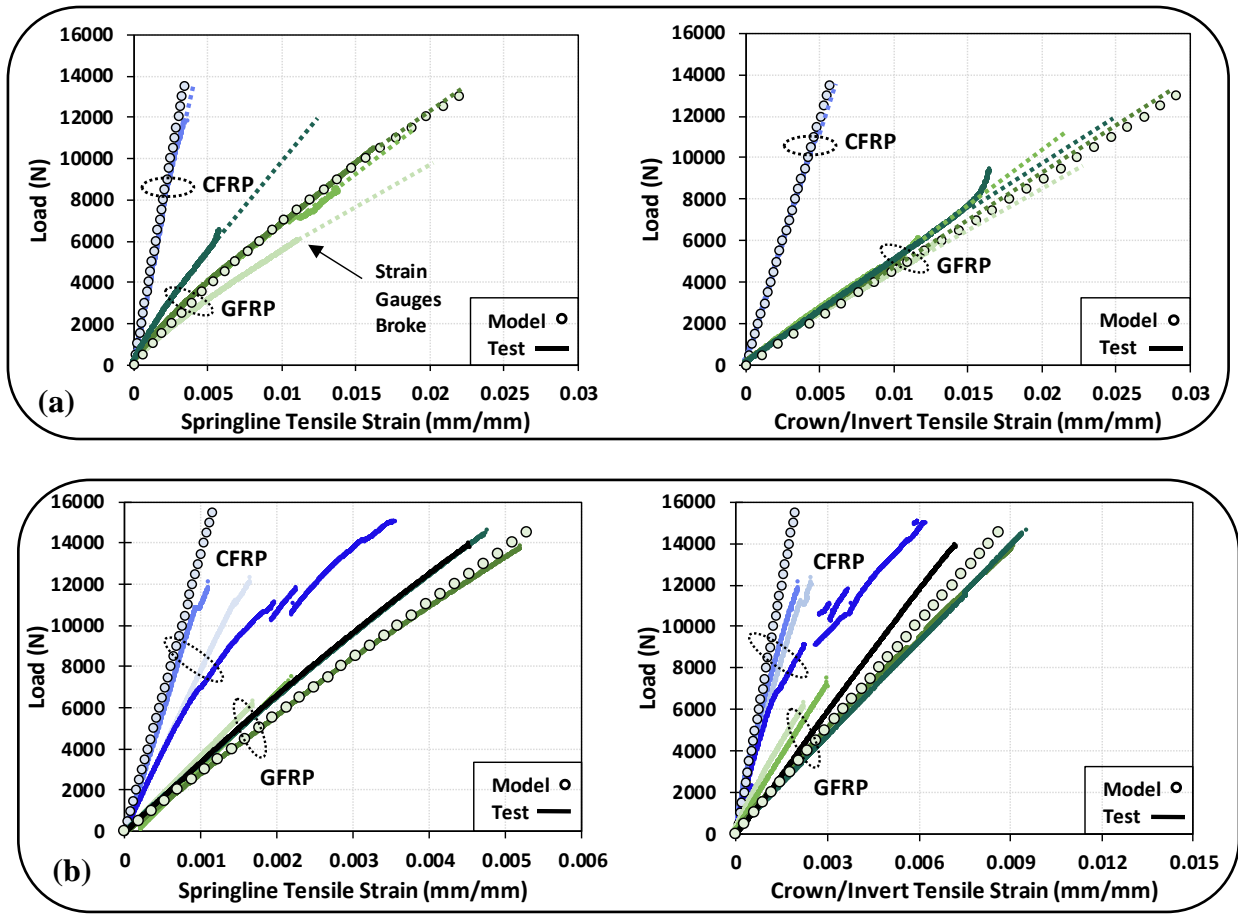


**Figure 13: Verification of analytical model based on load vs. strain: (a) solid-wall specimens; and (b) sandwich specimens with bulkermat core.**